WARSAW UNIVERSITY OF TECHNOLOGY Index 351733
FACULTY OF CIVIL ENGINEERING
COMMITTEE FOR CIVIL AND WATER ENGINEERING
POLISH ACADEMY OF SCIENCES ISSN 1230-2945

DOI: 10.24425/ace.2026.1414
ARCHIVES OF CIVIL ENGINEERING
Vol. LXXII ISSUE 3 2026

 pp. 541 –553

Research paper

Study on the influence of shield tunneling on the dynamic response of high-speed rail tunnel tracks

Ruizhen Fei[1], Limin Peng[2], Luo Zhang[3], Chunlei Zhang[4], Peng Zhang[5], Jiqing Zhang[6]

Abstract: In high-speed railway tunnels in China, shield tunneling often causes post-construction differential deformation, compromising driving safety and comfort. To address this, an integrated calculation model is developed, incorporating vehicles, tracks, tunnels, and surrounding rocks. The model evaluates the effects of cosine-shaped settlement deformation from shield tunneling on wheel-rail vertical force, wheel load reduction rate, and vehicle vertical acceleration, assessing train safety and comfort. The study examines three key factors: vertical clearance between shield tunneling and railway, horizontal angle of shield tunneling, and center distance of double-line shield tunnels. Results show that increasing vertical spacing enhances train safety and stability while reducing dynamic train-track interactions. Conversely, larger tunnel axis angles decrease safety and stability, with minimal additional impact beyond 50°. Increasing the horizontal spacing of double-line tunnels initially improves train safety and stability up to 24m, but further spacing reduces stability due to increased dynamic responses. These findings provide insights into optimizing shield tunneling parameters to ensure high-speed train operation safety and comfort in tunnel environments.

Keywords: shield tunneling, high-speed rail tunnel, integrated model of vehicle rail tunnel, post work deformation, driving comfort, driving safety

[1]PhD., Eng., 1) Central South University, School of Civil Engineering, Changsha, 410075, China, 2) China Railway Design Corporation, Tianjin, 300142, China, e-mail: ruizhenfei@yeah.net, ORCID: 0000-0002-9142-4890
[2]Prof., PhD., Central South University, School of Civil Engineering, Changsha, 410075, China, e-mail: lmpeng@mail.csu.edu.cn, ORCID: 0000-0002-0402-2368
[3]PhD., Eng., Central South University, School of Civil Engineering, Changsha, 410075, China, e-mail: feiruizhen@163.com, ORCID: 0009-0005-5495-4533
[4]MSc., Eng., China Railway Design Corporation, Tianjin, 300142, China, e-mail: zhangchunlei@crdc.com, ORCID: 0000-0002-0630-1467
[5]MSc., Eng., China Railway Design Corporation, Tianjin, 300142, China, e-mail: zhangpeng04@crdc.com, ORCID: 0000-0001-6185-2379
[6]MSc., Eng., China Railway Design Corporation, Tianjin, 300142, China, e-mail: zhangjiqing@crdc.com, ORCID: 0000-0002-0864-9934

1. Introduction

With the continuous development of urbanization, the phenomenon of shield tunneling in the area below existing high-speed railway tunnels has become frequent, and scholars at home and abroad have conducted in-depth research on such issues [1–3]. Liang et al. [4] analyzed the longitudinal deformation of existing shield tunnels caused by the underpass and double span construction of new shield tunnels using the Winkler foundation EB beam (Euler Bernoulli beam) model and the Winkler foundation T-beam (Timoshenko beam) model, respectively. Domestic and foreign scholars have conducted extensive research on the safety and stability of train operation. Cheng et al. [5] derived the vibration differential equation of railway vehicle motion on curves based on a linear creep model, and analyzed the influence of vehicle speed on safety and stability under different curve radii using linear and nonlinear models; Yau [6] studied the dynamic response of magnetic suspension trains running on guide rails with uneven settlement and found that even if the uneven settlement is small, there will be a significant amplification of the train's dynamic response at high speeds. RECUERO et al. [7] proposed a method that can effectively capture the mid frequency vehicle track interaction, contact plate elasticity, and vehicle dynamics laws. Ju et al. [8] studied the safety issues of a series of maglev trains under multi span bridge foundation settlement and earthquake action. Cheli et al. [9] analyzed the impact of track irregularities on vehicle vibration and found that excitation of different vibration modes has a significant impact on driving comfort.

In fact, when a train travels on the ground subgrade and in an underground tunnel, the vibration and stability of the vehicle also differ due to the different environments in which it operates. Currently, a large amount of research focuses on the dynamic response of tunnel structures and the vibration of the surrounding environment caused by subway operation. Representative models include Nejati et al.'s 2D model [10], Galv et al.'s 2.5D model [11], Forrest et al.'s "Pipe in Pipe" model [12], and Yang et al.'s shield tunnel vibration excitation model tests [13, 14]. However, there is little research on the safety and stability of subway operation. Currently, most research generally uses the unevenness spectrum of railway tracks as external excitation, ignoring the interaction between vehicles, tracks, shield tunnels, and surrounding rocks. The impact of adjacent excavation on existing shield tunnels and the safety and comfort of train operation are usually studied separately, which cannot reveal the impact of high-speed railway tracks on train operation after deformation caused by shield tunneling. Current domestic and international research on the impact of railway subgrade settlement primarily focuses on the stress analysis of track structures and deformation trend prediction. Studies utilize actual monitoring data and simulation algorithms to analyze the developmental trends of railway line deformation [15–17]. Some literature examines the effects of foundation deformation on railway track regularity, while other scholars have proposed control limits for differential settlement and remediation measures based on dynamic response indicators [18]. Although several researchers have investigated the dynamic responses of track and vehicle systems following deformations in roadbeds and bridges, there remains a significant lack of studies addressing the impact of tunnel foundation deformations on the vehicle-track system. The construction of shield tunnels can induce deformations in existing tunnels. These deformations transfer to track structures through interlayer interactions, resulting in geometric deviations of the track alignment. When trains pass through these affected sections, the wheel-rail interaction forces intensify, leading to track structure damage. This damage subsequently exacerbates wheel-rail interactions, creating a vicious cycle that accelerates the deterioration of both vehicles and track components. In severe cases, this process may compromise operational safety. Particularly for mountain tunnels, shield tunnel construction tends to cause greater soil disturbance due to complex geological conditions, potentially inducing deformations in existing tunnel foundations that significantly affect the vehicle-track-tunnel system. However, research investigating how different shield tunnel construction conditions influence this integrated system remains extremely limited.

Therefore, the author of this article takes the engineering case of settlement and deformation of existing high-speed railway lines caused by shield tunneling excavation as the research background, establishes an integrated model of vehicle rail tunnel surrounding rock, and conducts research on the safety and comfort of high-speed railway driving under the deformation of shield tunneling under high-speed railway tunnels. Furthermore, the influencing factors of driving safety and comfort are analyzed.

2. Project overview

2.1. Case overview

The shield tunnel between Xianglong Station and Xingsha Station on Changsha Metro Line 3 passes under the Liuyanghe Tunnel on the Beijing Guangzhou high-speed railway at DK34+856. The position relationship between the shield tunnel on Line 3 and the existing high-speed railway tunnel is shown in Fig. 1. The current situation of the underpass section of the interval shield tunnel is that the Liuyang River Tunnel is an entrance open cut tunnel section. The newly built shield tunnel axis in the underpass section has a burial depth of 32.61 m, a vertical clearance distance of 12.48 m from the existing tunnel lining, and a center distance of 15.0 m between the left and right tunnel lines.

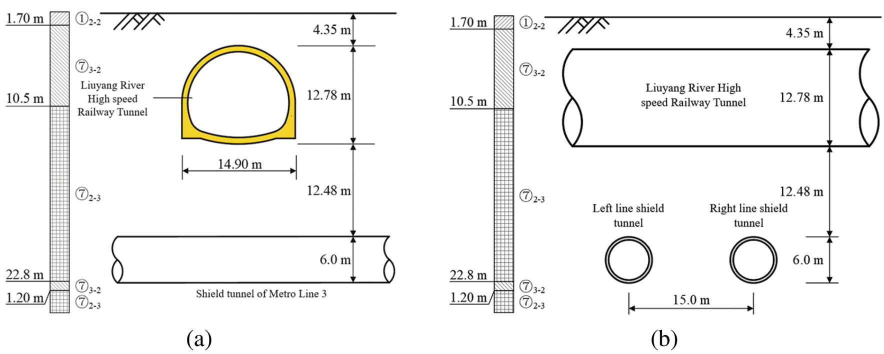

Fig. 1. The relative position relationship between the newly-built shield tunnel and the Liuyang River high-speed railway tunnel; (a) Vertical section, (b) Cross section

2.2. Determination of Basic Calculation Parameters

As shown in Fig. 1, the existing Liuyang River high-speed railway tunnel has a horseshoe shaped section. For ease of calculation, its section is equivalent to a circular section based on its cross-sectional area. The inner contour area of the horseshoe shaped section is about 120 m^2, so the equivalent section diameter is taken as 12.36 m, and the lining thickness is calculated based on the thickness of the arch crown, which is taken as 0.8 m. The tunnel lining adopts C35 reinforced concrete segments, so the elastic modulus is taken as 3.15×10^4 MPa, and the Poisson's ratio is taken as 0.2. Considering the influence of lining construction quality and segment structural joints, the stiffness of the lining is reduced to a certain extent during actual calculation. The reduction factor in this article is considered as 0.8, and the longitudinal equivalent bending stiffness and shear stiffness of the existing high-speed railway tunnel are finally obtained as 1.23×10^{10} kN·m^2 and 1.62×10^8 kN/m, respectively.

According to the geological survey data, the basic physical and mechanical parameters of the main strata within the calculated cross-section of the underpass section are shown in Table 1. When calculating, the geological parameters are calculated based on the weighted average of the thickness ratio of the geological layer within the calculation section. The rock and soil calculation parameters used are: elastic modulus of 900 MPa, Poisson's ratio of 0.25, weight of 22.9 kN/m^3, and internal friction angle of 31°. Due to the lack of detailed geological mechanics statistical parameters, it is assumed that the coefficient of variation of the stiffness of the underlying foundation of the existing tunnel is 0.3 during the calculation. When using random analysis method, the horizontal fluctuation distance of foundation stiffness is taken as 5D (D is the outer diameter of the newly built shield tunnel) as the basic working condition for research.

Table 1. Physical and mechanical parameters of geological strata

Stratum Number	Stratum Name	Heavy Weight (kN/m^3)	Internal friction angle (°)	Elastic modulus (MPa)	Poisson's ratio
12-2	Plain fill soil	19.7	15.6	13	0.3
73-2	Strongly weathered conglomerate	22.9	30.0	150	0.25
72-2	Moderately weathered mudstone sandstone	23.1	32.0	1300	0.22

According to the on-site construction plan, the tunnel between Xianglong Station and Xingsha Station on Metro Line 3 will be constructed using two earth pressure balance shield machines. The excavation diameter of the shield machine is 6.25 m, the length of the shield body is about 8.0 m, and the cutterhead is constructed with 4 main beams and 4 panels, with an opening rate of 37%. The construction parameters for the shield tunneling under the Liuyang River Tunnel of the Beijing Guangzhou high-speed railway determined based on the excavation construction of the experimental section are shown in Table 2, and the average of each parameter is taken for calculation.

Table 2. Construction parameters of shield tunneling through Liuyanghe Tunnel of Beijing Guangzhou High speed Railway

Parameters	Value	Parameters	Value
Soil storage pressure (bar)	0.8–1.2	Synchronous grouting volume (m^3)	6.9–7.1
Total thrust (MN)	11.5–12.5	Synchronous grouting pressure (MPa)	0.24–0.28
Knife disk torque (MN·m)	2.6–2.9	Excavated quantity (m^3)	60–62
Cutterhead speed (rpm)	1.4–1.6	Secondary grouting pressure (MPa)	0.3–0.5
Excavation speed (mm/min)	20–25	Secondary grouting volume (m^3)	1.0–1.4

3. Dynamic response analysis model of vehicle track tunnel structural system

The core content of the nonlinear dynamic analysis method for the vehicle track tunnel structural system mainly includes the establishment of the motion equation of the vehicle track tunnel system, model construction, and the selection of the optimal numerical integration method.

3.1. Construction Method for Dynamic Response Analysis Model of Structural System

According to Hamilton's principle of dynamics, the nonlinear dynamic equilibrium equation of a structural system is expressed as:

$$M\ddot{u} + C\dot{u} + Ku = F \tag{3.1}$$

In the formula: M – structural system quality matrix; C – Damping matrix of structural system; K – Structural system stiffness matrix; F – Load vector of structural system; u – Structural system node displacement vector; $\dot{u}$ – Velocity vector of structural system nodes; $\ddot{u}$ – Acceleration vector of structural system nodes.

Eq. (3.1) is the basic equation used to analyze the dynamic response of high-speed trains, such as displacement, acceleration, stress, and strain, under the coupling of static and dynamic loads in existing high-speed railway tunnels and underpass shield tunnels.

3.2. Integrated coupling model of vehicle rail tunnel

(1) Vehicle subsystem model

Given that the research focus is on the additional dynamic response characteristics of high-speed trains caused by the deformation of the lower structure and track structure of existing high-speed railway tunnels during shield tunneling construction, the following simplified assumptions are adopted to construct the vehicle subsystem calculation model:

1. Consider the entire vehicle as a rigid body, ignoring the elastic deformation of the vehicle wheelsets, bogies, and body;

2. Due to the insignificant impact of the lateral movement of the train on its vertical movement, the focus is on analyzing the vertical dynamic effects of vehicle buoyancy and nodding;

3. Not considering the longitudinal and transverse interaction forces between the wheel and rail of the vehicle, as well as the coupling effects between adjacent carriages.

The power equation of the vehicle subsystem is as follows:

$$M_v \ddot{u}_v + C_v \dot{u}_v + K_v u_v = F_v \tag{3.2}$$

In the formula: M_v – the mass matrix of the vehicle subsystem; C_v – damping matrix of vehicle subsystem; K_v – stiffness matrix of the vehicle subsystem; – Acceleration vector of vehicle subsystem; – Node velocity vector of vehicle subsystem; – Node displacement vector of vehicle subsystem; F_v – Node load vector of the vehicle subsystem.

The high-speed train adopts the CRH380 type car, which consists of one car body, two bogies, four wheelsets, seven rigid bodies, and one and two suspension systems. Spring and damping connections are used between the vehicle body and the bogie, as well as between the bogie and the wheelset. The high-speed train model established from this is shown in Fig. 2 inside the tunnel. The main calculation parameters of the vehicle model suspension system are shown in Table 3.

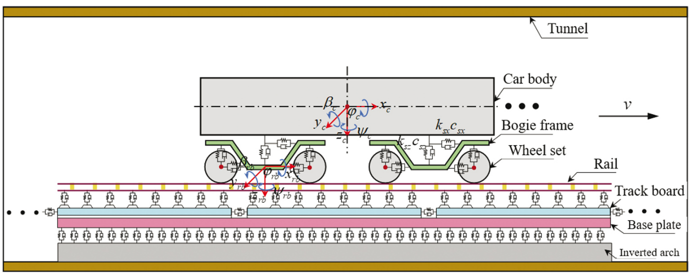

Fig. 2. Vehicle Model Diagram

Table 3. Calculation Parameters of Spring Stiffness and Damping of Vehicle Suspension System

Part	Spring stiffness (MN/m)			Spring Damping (kN·s/m)
Vertical	Horizontal	Longitudinal		
Primary suspension	0.55	5.0	10.0	6.0
Secondary suspension	0.40	0.15	0.15	80.0

(2) Model of ballastless track and inverted arch filling layer subsystem

The dynamics of the ballastless track and inverted arch filling layer subsystem are as follows.

$$M_t \ddot{u}_t + C_t \dot{u}_t + K_t u_t = F_t \tag{3.3}$$

Using three-dimensional solid elements to simulate the steel rail, ballastless track, and inverted arch filling layer system. The fasteners consider longitudinal, transverse, and vertical stiffness, and are simulated using the connectors provided by ABAQUS. The schematic diagram of ballastless track and inverted arch filling layer is shown in Fig. 3, the model diagram is shown in Fig. 4, and the relevant calculation parameters of the track structure are shown in Table 4.

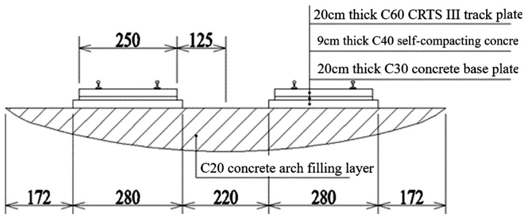

Fig. 3. Schematic diagram of track and filling layer (unit: cm)

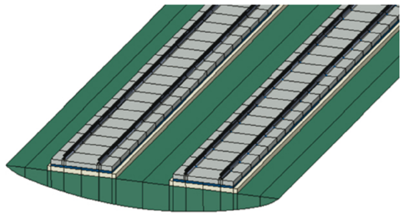

Fig. 4. Model diagram of track and filling layer

Table 4. Parameters of Track Structure

Parameter	Value
Elastic modulus of steel rail	2.059×10^{11} N/m^2
Inertia of rail section	3.217×10^{-5} m^4
Elastic modulus of roadbed	1.2×10^{8} Pa
Stiffness of rail pad adhesive	6.0×10^{7} N/m
Rubber damping pad under the rail	7.5×10^{4} N·s/m
Lateral stiffness of fasteners	30×10^{6} N/m
Lateral damping of fasteners	60×10^{3} N·s/m

(3) Subsystem model of high-speed rail tunnel and shield tunnel structure

The dynamic equation of the structural subsystem composed of high-speed rail tunnels, shield tunnels, and surrounding areas can be expressed as:

$$M_s\ddot{u}_s + C_s\dot{u}_s + K_s u_s = F_s \tag{3.4}$$

In the calculation model, the lining structure of high-speed rail tunnel formwork, shield tunnel segment lining, and surrounding rock are all simulated using three-dimensional solid elements. Both types of tunnel lining structures are considered as elastic materials; The surrounding rock of the tunnel is considered as an elastic-plastic material that follows the Mohr Coulomb criterion.

3.3. Modeling process

Based on the ABAQUS platform, the modeling process for establishing a vehicle track tunnel integrated model for high-speed railway tunnel dynamics analysis is shown in Fig. 5.

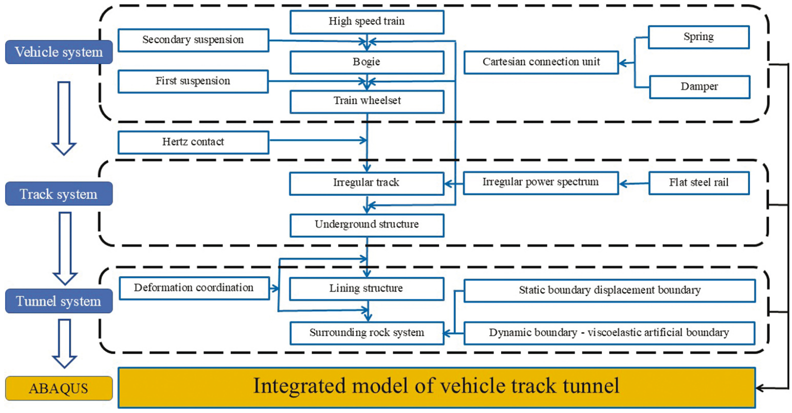

Fig. 5. Modeling Process of Vehicle Rail Tunnel Integrated Model

4. Dynamic response of high-speed railway tunnels at different spatial positions of shield tunneling

This section uses the finite element numerical calculation model of the vehicle track tunnel integration to analyze the dynamic response characteristics of the vehicle track system when a high-speed train passes through an existing high-speed railway tunnel under different vertical spacing, different angles of the shield tunnel axis, and different horizontal spacing conditions of the double line shield. Among them, six small working conditions are set for the vertical spacing of shield tunneling; Five small working conditions are set for the angle of the shield tunneling axis; Nine small working conditions are set at the horizontal spacing between the centers of two shield tunnels, as shown in Table 5 for details. Taking the vehicle speed as 350 km/h and the influence of track roughness, this study focuses on analyzing the characteristics of changes in indicators such as wheel rail vertical force, wheel load reduction rate, vertical acceleration of the vehicle body, and Spering index to investigate the impact of different operating conditions on the safety and stability of high-speed train operation.

Table 5. Calculation conditions of dynamic response of shield tunnel and high-speed rail tunnel at different spatial positions relative to each other

Vertical clearance distance (m)	Horizontal angle (°)	Shield spacing (m)	Notes
3	10	12	Formation loss rate 0.6%
6	30	18	Grouting thickness 0 m
9	50	24	—
12	70	30	—
15	90	36	—

Continued on next page

Table 5 – *Continued from previous page*

Vertical clearance distance (m)	Horizontal angle (°)	Shield spacing (m)	Notes
18	—	42	—
—	—	48	—
—	—	54	—
—	—	60	—

4.1. Vertical clear distance from high-speed rail tunnel

Based on engineering cases, the center distance of the double track is taken as 24 m, and the horizontal angle with the high-speed rail tunnel is 90°.

(1) Wheel rail vertical force and wheel load reduction rate

Figs. 6(a) and 6(b) respectively show the time history curves of the wheel rail dynamic interaction and vertical vibration acceleration of high-speed vehicles passing through the settlement zone of a double track tunnel under the influence of different tunnel vertical spacing. It can be seen from the two figures that:

1. The dynamic response of high-speed trains in tunnels with a vertical spacing of 3m is slightly greater than that in tunnels with a spacing of 18 m. When the vehicle passes through the settlement area of the tunnel, the vertical force between the wheel and rail varies between 40 kN and 110 kN, with little fluctuation amplitude, and the wheel weight also fluctuates back and forth during the process of load reduction and loading;

2. The values of vertical wheel rail force and wheel load reduction rate under various operating conditions do not change significantly, and the waveforms of single track tunnel and double track tunnel under various operating conditions are similar. Therefore, the time history of vertical wheel rail force and wheel load reduction rate under various operating conditions in single track tunnel will not be provided.

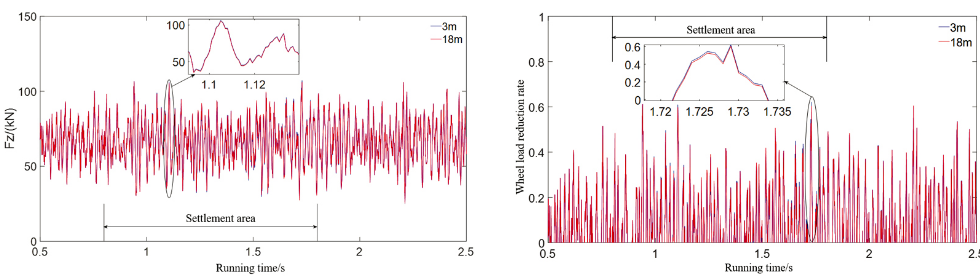

Fig. 6. Time history of wheel rail vertical force/wheel load reduction rate under the influence of vertical clearance in a double track tunnel; (a) Vertical wheel rail force time history, (b) Time history of wheel load reduction rate

Fig. 7 shows the power spectral density of vertical force between the wheel and rail under different working conditions in single track and double track tunnels. It can be seen from the figure that increasing the vertical spacing between tunnels will significantly reduce the power spectral density of vertical force within 5 Hz, improving the smoothness of driving.

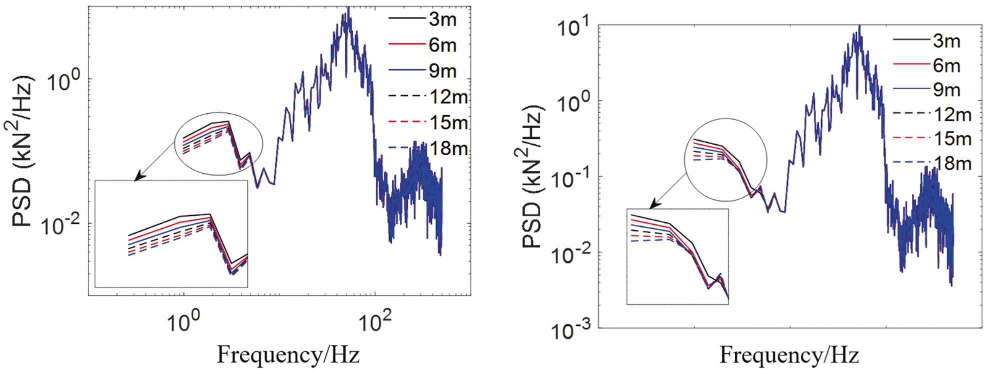

(a) (b)

Fig. 7. Power spectrum of wheel rail vertical force under the influence of different vertical clearances in tunnels; (a) Single line tunnel working condition, (b) Double line tunnel working conditions

Fig. 8 shows the effect of different tunnel vertical spacing on the vertical acceleration of the vehicle body when a high-speed train passes through an uneven tunnel settlement area at a speed of 350 km/h under single and double track tunnel conditions. It can be seen from the figure that increasing the tunnel vertical spacing has a reducing effect on the vertical acceleration of the vehicle body. During the process of increasing the tunnel vertical spacing from 3 m to 18 m, the vertical acceleration of the vehicle body in the settlement area slightly decreases.

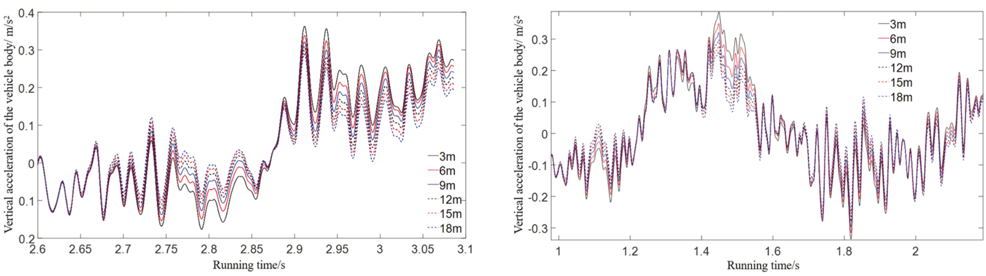

(a) (b)

Fig. 8. Time history curve of vertical acceleration of the vehicle body under the influence of different vertical clearances in the tunnel; (a) Single line tunnel working condition, (b) Double line tunnel working conditions

(2) Vertical acceleration and Sperling index

Figs. 9(a) and 9(b) are the graphs of the maximum vertical acceleration and Sperling index changes of the vehicle body under different vertical spacings in single track and double track tunnels, respectively. It can be seen from the graphs that, regardless of the working conditions in single track and double track tunnels, as the vertical spacing of the tunnel increases, the vertical acceleration and Sperling index of the vehicle body decrease. Therefore, increasing the vertical spacing of the tunnel appropriately can improve the stability of driving. The change curves of each indicator are similar, and the amplitude of the change is not large. The maximum vertical acceleration of the vehicle body under various working conditions in single track and double track tunnels does not exceed the limit value. However, in single track tunnels, the vertical spacing of the tunnel is less than 9 m, and in double track tunnels, the tunnel spacing is less than 12 m. The vertical Spering index has exceeded 3, exceeding the limit of the qualified level for passenger cars in the “Test and Identification Specification”, It is suggested to increase the vertical spacing of tunnels appropriately to improve the safety and stability of driving.

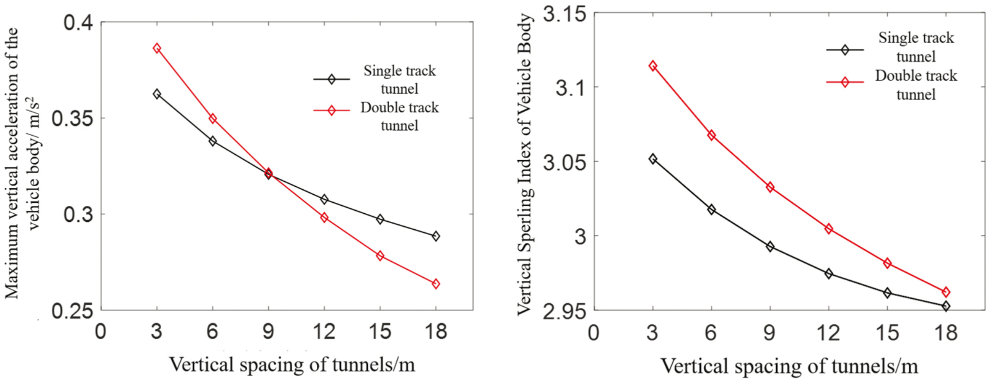

(a) (b)

Fig. 9. Maximum vertical acceleration/Spering index of the vehicle body under the influence of the vertical clearance of the tunnel; (a) Maximum vertical acceleration of the vehicle body under various operating conditions, (b) Maximum vertical Spering index of the vehicle body under various operating conditions

4.2. Horizontal angle with high-speed rail tunnel

Based on engineering cases, analyze the dynamic response characteristics of trains under different angles between the central axis of shield tunnels and the central axis of high-speed rail tunnels as listed in Table 5. The center distance of the double track is taken as 24 m, and the vertical distance from the high-speed rail tunnel is taken as 12 m.

As shown in Figs. 10(a) to 10(b), the time history curves of the wheel rail dynamic interaction and the vertical vibration acceleration of the vehicle body at the center of mass caused by the high-speed vehicle passing through the settlement zone of the double track tunnel under the influence of different tunnel axis angles are presented. It can be seen from the figures that the dynamic response of the high-speed train at a tunnel axis angle of 90° is slightly greater than that at a tunnel axis angle of 0°. When the vehicle passes through the settlement zone of the tunnel, the vertical force of the wheel rail varies between 30 kN and 110 kN, and the fluctuation amplitude is not large. The wheel load is first reduced and then loaded. The values of the wheel rail vertical force and the wheel load reduction rate do not change much under various working conditions, and the waveforms of the single track tunnel and double track tunnel are similar under various working conditions. Therefore, it is no longer necessary to... Provide the time history of vertical wheel rail forces and wheel load reduction rates under various operating conditions in a single track tunnel.

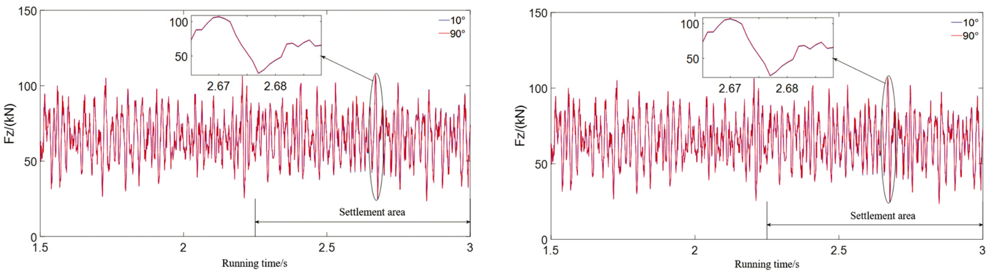

(a) (b)

Fig. 10. Time history of wheel rail vertical force/wheel load reduction rate under the influence of tunnel axis angle in a double track tunnel; (a) Vertical wheel rail force time history, (b) Time history of wheel load reduction rate

5. Conclusions

This study establishes a vehicle-ballastless track-tunnel coupling dynamic model to investigate the impact of shield tunneling parameters on high-speed rail operations. Key dynamic responses, including wheel load reduction rate, vehicle acceleration, wheel-rail vertical force, and Sperling index, were analyzed under various conditions. The results indicate that tunnel uplift deformation within standard control limits ensures operational safety but affects train comfort. Increasing the vertical spacing of shield tunneling enhances safety, stability, and reduces dynamic noise, while larger tunneling axis angles decrease safety and stability, particularly beyond 50°. For double-line shield tunnels, increasing the horizontal distance initially improves safety and stability but diminishes them when exceeding 24 m. These findings provide a comprehensive understanding of how shield tunneling parameters influence the safety, comfort, and stability of high-speed rail operations, offering valuable guidance for optimizing tunnel design and construction.

References

[1] R. Liang, "Simplified analytical method for evaluating the effects of overcrossing tunnelling on existing shield tunnels using the nonlinear Pasternak foundation model", *Soils and Foundations*, vol. 59, no. 6, pp. 1711–1727, 2019, doi: 10.1016/j.sandf.2019.07.009.

[2] R. Fei, L. Peng, C. Zhang, J. Zhang, and P. Zhang, "Centrifuge model test of parallel shield underneath high-speed railway tunnel", *Archives of Civil Engineering*, vol. 68, no. 3, pp. 661–677, 2022, doi: 10.24425/ace.2022.141909.

[3] R. Fei, L. Peng, C. Zhang, J. Zhang, and P. Zhang, "Mechanical characteristics of twin tunnel underneath construction on existing high-speed railway tunnel", *Archives of Civil Engineering*, vol. 69, no. 1, pp. 403–420, 2023, doi: 10.24425/ace.2023.144180.

[4] R. Liang, T. Xia, Y. Hong, and F. Yu, "Effects of above-crossing tunnelling on the existing shield tunnels", *Tunnelling and Underground Space Technology*, vol. 58, pp. 159–176, 2016, doi: 10.1016/j.tust.2016.05.002.

[5] Y.C. Cheng and C.T. Hsu, "Running safety and comfort analysis of railway vehicles moving on curved tracks", *International Journal of Structural Stability and Dynamics*, vol. 14, no. 4, art. no. 1450004, 2014, doi: 10.1142/S0219455414500047.

[6] J.D. Yau, "Response of a maglev vehicle moving on a series of guideways with differential settlement", *Journal of Sound and Vibration*, vol. 324, no. 3-5, pp. 816–831, 2009, doi: 10.1016/j.jsv.2009.02.031.

[7] A.M. Recuero and J.L. Escalona, "Dynamics of the coupled railway vehicle-flexible track system with irregularities using a multibody approach with moving modes", *Vehicle System Dynamics*, vol. 52, no. 1, pp. 45-67, 2014, doi: 10.1080/00423114.2013.857030.

[8] S.H. Ju, C.C. Leong, and Y.S. Ho, "Safety of maglev trains moving on bridges subject to foundation settlements and earthquakes", *Journal of Bridge Engineering*, vol. 19, no. 1, pp. 91–100, 2014, doi: 10.1061/(ASCE)BE.1943-5592.0000506.

[9] F. Cheli and R. Corradi, "On rail vehicle vibrations induced by track unevenness: Analysis of the excitation mechanism", *Journal of Sound and Vibration*, vol. 330, no. 15, pp. 3744–3765, 2011, doi: 10.1016/j.jsv.2011.02.025.

[10] H.R. Nejati, M. Ahmadi, and H. Hashemolhosseini, "Numerical analysis of ground surface vibration induced by underground train movement", *Tunnelling and Underground Space Technology*, vol. 29, pp. 1–9, 2012, doi: 10.1016/j.tust.2011.12.006.

[11] P. Galvín, S. François, M. Schevenels, E. Bongini, G. Degrande, and G. Lombaert, "A 2.5 D coupled FE-BE model for the prediction of railway induced vibrations", *Soil Dynamics and Earthquake Engineering*, vol. 30, no. 12, pp. 1500–1512, 2010, doi: 10.1016/j.soildyn.2010.07.001.

[12] J.A. Forrest and H.E.M. Hunt, "Ground vibration generated by trains in underground tunnels", *Journal of Sound and Vibration*, vol. 294, no. 4-5, pp. 706–736, 2006, doi: 10.1016/j.jsv.2005.12.031.

[13] W. Yang, G. Cui, Z. Xu, Q. Yan, C. He, and Y. Zhang, "An experimental study of ground-borne vibration from shield tunnels", *Tunnelling and Underground Space Technology*, vol. 71, pp. 244–252, 2018, doi: 10.1016/j.tust.2017.08.020.

[14] W. Yang, et al., "An experimental study of the dynamic response of shield tunnels under long-term train loads", *Tunnelling and Underground Space Technology*, vol. 79, pp. 67–75, 2018, doi: 10.1016/j.tust.2018.04.031.

[15] Y. Guo and W. Zhai, "Long-term prediction of track geometry degradation in high-speed vehicle-ballastless track system due to differential subgrade settlement", *Soil Dynamics and Earthquake Engineering*, vol. 113, pp. 1–11, 2018, doi: 10.1016/j.soildyn.2018.05.024.

[16] H. Wang and V. Markine, "Modelling of the long-term behaviour of transition zones: Prediction of track settlement", *Engineering Structures*, vol. 156, pp. 294–304, 2018, doi: 10.1016/j.engstruct.2017.11.038.

[17] Y. Shan, et al., "Iterative method for predicting uneven settlement caused by high-speed train loads in transition-zone subgrade", *Transportation Research Record*, vol. 2607, no. 1, pp. 7–14, 2017, doi: 10.3141/2607-02.

[18] X. Zhang, M. Burrow, and S. Zhou, "An investigation of subgrade differential settlement on the dynamic response of the vehicle-track system", *Proceedings of the Institution of Mechanical Engineers, Part F: Journal of Rail and Rapid Transit*, vol. 230, no. 7, pp. 1760–1773, 2016, doi: 10.1177/0954409715613538.

Received: 2024-12-17, Revised: 2025-04-04